Journal of Colloid and Interface Science 672 (2024) 797–804

Contents lists available at ScienceDirect

Journal of Colloid And Interface Science

journal homepage: www.elsevier.com/locate/jcis

Regular Article

Modulating the conformation of microgels by complexation with inorganic nanoparticles

Jacopo Vialetto [a,b,c,*], Shivaprakash N. Ramakrishna [b], Sebastian Stock [d], Regine von Klitzing [d], Lucio Isa [b]

[a] Department of Chemistry "Ugo Schiff", University of Florence, via della Lastruccia 3, 50019 Sesto Fiorentino (FI), Italy
[b] Laboratory for Soft Materials and Interfaces, Department of Materials, ETH Zürich, Vladimir-Prelog-Weg 5, 8093 Zürich, Switzerland
[c] Consorzio interuniversitario per lo sviluppo dei Sistemi a Grande Interfase (CSGI), via della Lastruccia 3, 50019 Sesto Fiorentino (FI), Italy
[d] Institute for Condensed Matter Physics, Technische Universität Darmstadt, Hochschulstraße 8, 64289 Darmstadt, Germany

GRAPHICAL ABSTRACT

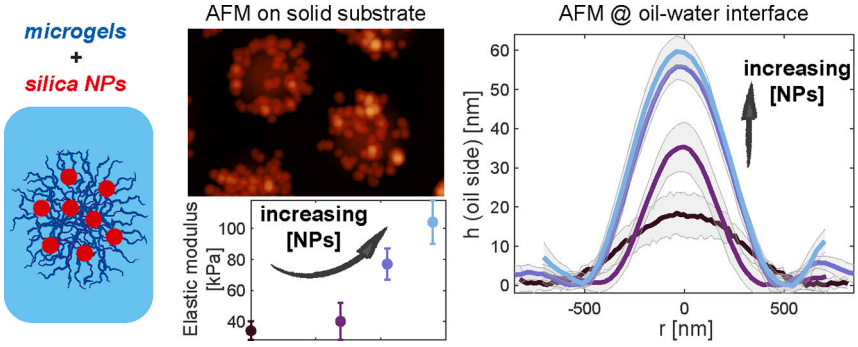

ARTICLE INFO

Keywords:
Hybrid microgel
Atomic force microscopy
Fluid interface
Colloidal particle
Hydrophobicity
Mechanical properties

ABSTRACT

Hypothesis: The complexation of microgels with rigid nanoparticles is an effective way to impart novel properties and functions to the resulting hybrid particles for applications such as in optics, catalysis, or for the stabilization of foams/emulsions. The nanoparticles affect the conformation of the polymer network, both in bulk aqueous environments and when the microgels are adsorbed at a fluid interface, in a non-trivial manner by modulating the microgel size, stiffness and apparent contact angle.

Experiments: Here, we provide a detailed investigation, using light scattering, *in-situ* atomic force microscopy and nano-indentation experiments, of the interaction between poly(N-isopropylacrylamide) microgels and hydrophobized silica nanoparticles after mixing in aqueous suspension to shed light on the network reorganization upon nanoparticle incorporation.

Findings: The addition of nanoparticles decreases the microgels' bulk swelling and thermal response. When adsorbed at an oil-water interface, a higher ratio of nanoparticles influences the microgel's stiffness as well as their hydrophobic/hydrophilic character by increasing their effective contact angle, consequently modulating the monolayer response upon interfacial compression. Overall, these results provide fundamental understanding on the complex conformation of hybrid microgels in different environments and give inspiration to design new materials where the combination of a soft polymer network and nanoparticles might result in additional functionalities.

* Corresponding author.
E-mail address: jacopo.vialetto@unifi.it (J. Vialetto).

https://doi.org/10.1016/j.jcis.2024.05.163
Received 9 January 2024; Received in revised form 16 May 2024; Accepted 21 May 2024
Available online 28 May 2024

1. Introduction

Microgels are highly investigated model colloidal particles due to their fast and reversible response to multiple stimuli, such as: temperature [1,2], pH [3], light [4], or in the presence of specific molecules [5,6]. This stimuli trigger the ability of the microgel's internal polymer network to incorporate solvent and swell, therefore modulating the particle size and elastic modulus [7–9], as well as the particle surface properties and resulting colloidal stability. As a consequence, they find numerous potential applications in diverse fields where their tunability is advantageous, e.g., for the fabrication of photonic crystals, the realization of drug delivery systems, as viscosity modifiers and biocatalysts [10].

In order to increase further the stimulus responsiveness of such "smart" colloids, several works investigated the complexation of microgels with rigid nanoparticles (NPs) [11,12]. The resulting hybrid complexes can be obtained either by an *in-situ* synthesis of the NPs inside already formed microgels, or by post-modification by NP adsorption and incorporation. The former approach has been reported for a variety of NPs, including metals, metal oxides, other inorganic materials and polymers [13–17]. The second route consists in embedding preformed NPs inside the microgels exploiting attractive interactions between the NPs surface and the polymeric network [8,18–21]. This method might provide a lower NP loading with respect to the *in-situ* synthesis, however it does not require additional synthesis steps and can be performed with NPs of any size and shape. Nanoparticle incorporation primarily imparts novel properties and functionalities to the microgels, yielding hybrid systems with plasmonic or magnetic properties, catalytic activity, selective light absorption, etc. [8,15,18,22]. Additionally, it might influence the relaxation of the polymeric network in the solvent, consequently modulating the particle size, swelling ratio and stimulus responsiveness [8,14,18,20,23]. In dense suspensions, the interaction between rigid and soft particles can also be used as an effective way to tune the rheological and thermogelling behavior of the samples under shear [24,25].

Microgels are also widely used as components to stabilize fluid interfaces, e.g., within foams, emulsions and colloidosomes [26]. In this context, the addition of NPs interacting with the microgel network can be used as a convenient way not only to expand their response to a large variety of external stimuli, but also to alter the microgels' hydrophilic/hydrophobic balance. This option enables tailoring the type of emulsion (oil-in water or water-in-oil emulsions) [27,28], and enhancing the mechanical properties of particle-laden interfaces [29,30]. Furthermore, the complexation of biologically relevant microgels (e.g., proteins and polysaccharides) with rigid particles, and their interaction with fluid interfaces, is also the subject of numerous studies for the production of food-grade materials [31].

Up to now, most research on hybrid microgels at fluid interfaces has focused either on hybrids obtained by *in-situ* synthesis [27,29,32], or by complexation directly at the interface following interactions between the components originally dispersed in the two separate phases [28,30,33]. Additionally, few works investigated in detail how the incorporation of NPs affects the microgels conformation, internal elasticity and resulting wetting behavior, mainly by using indirect measurements such as the contact angle of drops on deposited particle beds [32,33].

Here, we instead consider a simpler route, where complexes formed between poly(N-isopropyl-acrylamide) (pNIPAM) microgels and hydrophobized silica NPs are initially obtained in a single fluid phase (a water/ethanol mixture acting as bad solvent for pNIPAM) [7,34–36], and later adsorbed at a water/oil interface. We specifically provide a comprehensive study linking the polymer network relaxation in bulk upon NP loading with the single-particle conformation after adsorption at a fluid interface. We first characterize the complexes at low NPs content in bulk suspension by dynamic light scattering (DLS) to infer on the network swelling and resulting thermal response as a function of NPs concentration. We then adsorb the hybrid microgels at higher NPs ratio at a fluid interface, in order to investigate how the presence of NPs modulates the internal microgel stiffness, swelling extent and interfacial reorganization. DLS and nano-indentation experiments on deposited microgels provide insight onto the network elasticity upon NP loading. Additionally, *in-situ* atomic force microscopy (AFM) [37,38] is used to visualize for the first time the three-dimensional (3D) conformation of such complex objects when adsorbed at the oil-water interface, and allows quantifying the increase in microgel's hydrophobicity as a function of NPs incorporation. Finally, we exploit the modification of the single-particle stiffness to vary the mechanical properties of microgel monolayers subjected to compression on a Langmuir trough.

2. Materials and methods

2.1. Materials

N,N'-Methylenebis(acrylamide) (BIS, Fluka 99.0%), methacrylic acid (MAA; Acros Organics, 99.5%), potassium persulfate (KPS, Sigma–Aldrich 99.0%), ethanol (Fisher Chemical, 99.97%), isopropanol (Fisher Chemical, 99.97%), toluene (Fluka Analytical, 99.7%), n-hexadecane (Acros Organics 99.0%), n-hexane (SigmaAldrich, HPLC grade 95%) and octadecyltrimethoxysilane (ABCR GmbH, 97%) were used without further purification. N-isopropylacrylamide (NIPAM, TCI 98.0%) was purified by recrystallization in 40/60 v/v toluene/hexane.

Microgels synthesis. The synthesis of the microgels used in this study followed an already published procedure [39]. Specifically, the monomers (NIPAM and 5 mol% MAA) and the crosslinker (1 mol% BIS) were dissolved in MilliQ water. The solution was then purged with nitrogen for 1 h and heated up to 80° C. The reaction was started upon addition of 0.5 mol% of KPS (previously dissolved in MilliQ water and purged with nitrogen), and carried out for 6 h in a sealed flask. The microgels were then purified by dialysis for a week and 8 centrifugation cycles to remove the supernatant and redisperse the particles in pure water.

Silica nanoparticles surface modification. Commercially available silica nanospheres (Ludox TM40, Sigma Aldrich, Darmstadt) were hydrophobized using octatrimethytrimethoxysilane by using the same procedure reported in previous works [28,40]. Prior to use, the silica particles were cleaned by dialysis against at least 50 L of Milli-Q water. The silica particles were then diluted to 1 wt% in ethanol and 100 mL of the silica particle/ethanol dispersion was mixed with 250 μL of octadecyltrimethoxysilane. The reaction was carried out in ethanol under constant stirring for 1 h at room temperature and for another hour at 60 °C. The particles were then purified by centrifugation and redispersed in pure ethanol.

About 100 μL of 1 wt% particle dispersion was dried out on a 1.5x1.5 cm silicon wafer and the contact angle of a water drop on the obtained dry particle layer was checked to prove a successful hydrophobization. The measured contact angle was 110 ± 10°. The mean diameter of the particles was determined by TEM to be 26 ± 4 nm; therefore, surface modification did not affect the size of the particles. The zeta potential of the particles (- 45 ± 5 mV) was determined with a zetasizer (Malvern, UK).

2.2. Methods

Preparation of hybrid microgels. Microgels and silica NPs were initially dispersed in water and ethanol, respectively. The two components were then mixed in the required amount, measured as weight fraction of NPs with respect to the weight of the microgels, at a final ethanol volume fraction of $\xi_{EtOH} = 0.25$, by injecting the NPs into the microgel suspension. We note that a minimum amount of ethanol is required to avoid instantaneous aggregation of the NPs in water. The total volume was typically 1-2 mL, and the microgel concentration varied from 0.07 to 0.0007 wt%. The mixtures were then homogenized by shaking

for a total time of 20 min before starting each experiment. We note that all samples containing microgels (with or without NPs) were never sonicated. For dynamic light scattering (DLS) measurements in water, ethanol from the samples thus prepared was let to evaporate under vacuum at 40°C for at least 4 h, replacing from time to time the evaporate solvent with pure water.

DLS. DLS experiments were performed using a Zetasizer (Malvern, UK). Before each measurement, the desired temperature was let to equilibrate for 10 minutes. The correlation function of the obtained scattered intensity is fitted with the cumulant analysis performed by the instrument software. The resulting z-average sizes are reported in Table 1.

Langmuir-Blodgett technique. Microgel assembly at the fluid interface and concurrent deposition on silicon wafers at controlled surface pressure values (Π) were performed using a custom-built KSV5000 Langmuir trough made of a Teflon bath and Delrin barriers, following already published protocols [41–43]. The main details are summarized below. The silicon wafers were cleaned by 15 min ultrasonication in toluene, isopropanol, acetone, ethanol and Milli-Q water, and for additional 10 min in a UV-Ozone cleaner (UV/Ozone Procleaner Plus, Bioforce Nanosciences) just before starting the experiments. This procedure ensures a highly hydrophilic surface. A silicon wafer was then placed on a motorized arm inside the Teflon trough into the water phase at a 30° angle with respect to the water surface, prior to gently adding 120 mL of n-hexane to cover the water interface. The microgel suspension, freshly made before each experiment, was composed of a mixture of Milli-Q water and ethanol (4:1 ratio by volume) containing the desired amount of NPs and microgels, and was let to equilibrate for 10 minutes prior to injection at the hexane-water interface. After injection, the system was let to equilibrate for other 15 minutes. Then the compression-deposition experiment started: the barriers moved from a fully-open position (maximum area of 197.5 cm^2) to compress the interface at a constant speed of 2.3 $mm \cdot min^{-1}$, while the substrate was lifted up at a constant speed of 0.3 $mm \cdot min^{-1}$. Barriers and substrate speed were adjusted such as the substrate would be out of the water phase just before the compression finished. During the experiment, we recorded the surface pressure with a platinum Wilhelmy plate kept in a vertical position parallel to the barriers.

The microgel + NPs complexes transferred on the solid substrate were analyzed using AFM in tapping mode. The particle's conformation was obtained from transfers at low surface pressure values ($\Pi \simeq 5\ mN \cdot m^{-1}$), when the particles are non interacting, or only slightly interacting, at the fluid interface. The number of microgels on the substrate as a function of Π was calculated imaging the substrate every 500 μm from the initial position of the three-phase contact line to the end of the substrate. Knowing the dipper speed, we assigned to each AFM image the corresponding Π value measured during the compression experiment.

AFM Imaging. In-situ atomic force microscopy imaging of particles adsorbed at the oil-water interface was performed with a Bruker Dimension Icon AFM, following a procedure already reported elsewhere [37,38], using PeakForce tapping mode and cantilevers with a nominal spring constant of $\sim 0.12\ N \cdot m^{-1}$ (PEAKFORCE-HIRS-F-B, Bruker). The subphase was confined within a small well made of UV-curable glue (Norland Optical Adhesive 81) having an average depth of around 10 μm. We note that such a shallow well significantly mitigates drift of the scanner due to the solvent flows during AFM scanning. Deeper wells do not allow for an accurate AFM imaging of the microgels adsorbed at the fluid interface due to significant drift [37]. The aqueous subphase was composed of a mixture of Milli-Q water and ethanol (4:1 ratio by volume), containing the desired amount of microgels and NPs. The subphase was first loaded in the cell, and then covered with a layer of hexadecane (oil phase). All measurements were recorded at room temperature (22 ± 1°C). A minimum waiting time of 1 h was set in order to equilibrate the ethanol exchange between the aqueous and the oil phase, and for the arrest of any surface flow after loading. After equilibration, the AFM tip is gently approached to the interface from the oil side by setting a PeakForce set point of 100 pN, and adjusted slightly along with the feedback gains once the tip was engaged at the interface. The PeakForce during imaging was then varied between 100 - 500 pN in order to obtain high-quality images. The deliberate use of very low applied force in PeakForce Tapping mode allows us to maintain contact with the interface without breakage. Applying higher forces could potentially break the delicate interface, causing the tip to sink inside; this can be easily detected by a drop in the total laser intensity (SUM signal), ultimately leading to the loss of feedback control.

AFM of particles deposited on solid substrates by using the Langmuir-Blodgett technique was performed with the same instrument in tapping mode, using cantilevers with a nominal spring constant of $\sim 26\ N \cdot m^{-1}$ and resonance frequency of ~ 300 kHz (AC160TS-R3, Olympus Cantilevers, Japan).

Image analysis. All AFM images were first processed with the open-source software Gwyddion to correct for line and plane tilting and successively analyzed with custom MATLAB codes. The height profiles for each condition are obtained by averaging horizontal and vertical profiles passing through the centers of at least ten microgels, after alignment of all the profiles by their center value.

Nano-indentation. The elastic modulus was extracted from force versus indentation experiments obtained with an Asylum Research MFP 3D AFM (Oxford Instruments, Santa Barbara, CA). A silica microparticle (diameter = 2 μm, Microparticles GmbH) was used as indenter, attached to the end of a tipless cantilever using a two-component epoxy glue (UHU Plus endfest, UHU GmbH, Germany) with a home-built micromanipulator. The measurements were done in Milli-Q water at 25°C on microgels deposited from the hexane-water interface onto silicon wafers. The normal spring constant of the Au-coated cantilever (CSC-38, Mikromash, Bulgaria) was determined using the thermal-noise method [44] and is found to be 0.25 $N \cdot m^{-1}$. The force-vs-distance curves were recorded using the force-mapping mode over a $10 \cdot 10\ \mu m^2$ area and converted to force versus indentation. The obtained force-vs-indentation curves were then fitted with the Hertz model to extract the elastic modulus [7,8,43]. Examples for force-vs-indentation curves are shown in Figure S3. Since deposited microgels show a decrease in polymer layer thickness from the center to the edge of the particle, only the indentation curves recorded at the center of the microgels were analyzed in order to avoid any substrate effects on the particle periphery.

SEM Imaging. Scanning electron microscopy (SEM, Gemini Leo-1530, Germany) was performed on samples prepared by using the Langmuir-Blodgett technique, after coating with 10 nm Pt using a sputter coater (CCU-010, safematic GmbH, Switzerland).

Thermogravimetric analysis. Thermogravimetric analysis (TGA, TA Instruments, Discovery SDT 650) was performed using the following protocol: samples (approximately 20 mg) were heated up at 10°C/min from room temperature to 120°C, while recording the weight % loss as a function of temperature.

3. Results and discussion

We first investigated the complexation between pNIPAM microgels and hydrophobized silica NPs (diameter 26 ± 4 nm) by DLS (Fig. 1) in order to quantify the resulting microgel's hydrodynamic diameter (d) as a function of NPs addition. Microgels and silica NPs are initially dispersed in water and ethanol, respectively. Successively, the two components are mixed in the desired amount in water/ethanol mixtures at a final ethanol volume fraction of $\xi_{EtOH} = 0.25$ (note that a minimum amount of ethanol is required to avoid instantaneous aggregation of the NPs in water). The hydrodynamic diameter of the pure microgels at $\xi_{EtOH} = 0.25$ ($d^0_{et} = 250 \pm 5$ nm, see Table 1) shows the expected network collapse due to the co-nonsolvency effect commonly observed at this ξ_{EtOH} [7,34–36]. Consequently, when the NPs are successively added to the mixture, they interact with a collapsed pNIPAM network dispersed in a bad solvent, which drives their aggregation onto the poly-

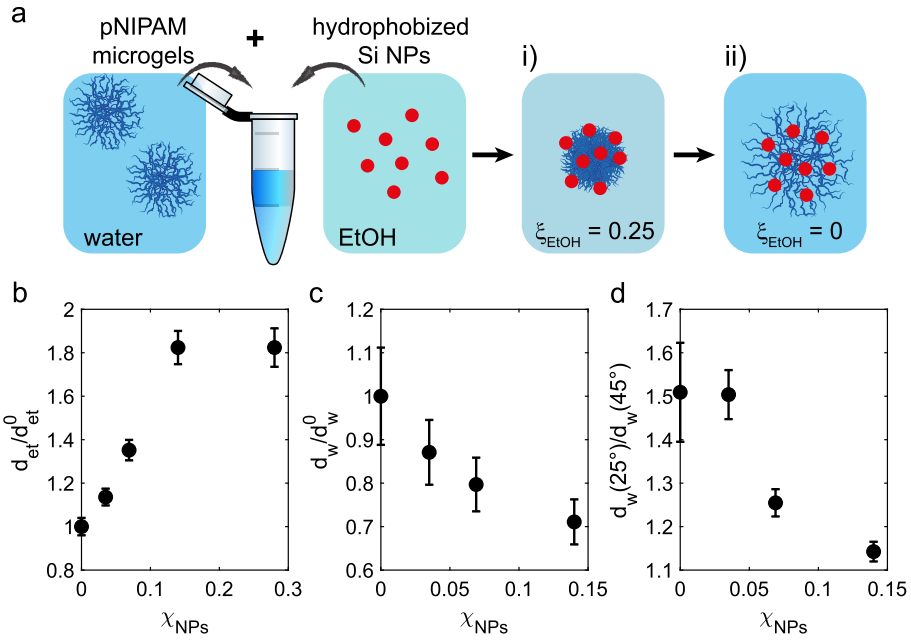

Fig. 1. a) Schematic of the sample preparation. Microgels and silica NPs, originally dispersed in water and ethanol, respectively, are mixed in water/ethanol mixtures at a final volume fraction of $\xi_{EtOH} = 0.25$ (i). Ethanol is then evaporated out from the suspension (ii). b) Relative microgels' hydrodynamic diameter d_{et} in water/ethanol mixtures ($\xi_{EtOH} = 0.25$) at 25°C as a function of NP concentration in weight fraction (χ_{NPs}), divided by the microgels size in the absence of NPs (d^0_{et}). c) Relative microgel diameter d_w in water at 25°C as a function of NP concentration, divided by the microgel size in water in the absence of NPs (d^0_w). d) Microgel deswelling ratio in water, measured as $d_w(25°C)/d_w(45°C)$.

Table 1
Experimental particle dimensions.

χ_{NPs}	d_{et} (25°C) [nm]	d_w (25°C) [nm]	d_w (45°C) [nm]
0	250 ± 5	1160 ± 65	770 ± 15
0.035	284 ± 4	1012 ± 30	673 ± 9
0.069	338 ± 5	926 ± 20	738 ± 6
0.14	456 ± 10	826 ± 14	723 ± 6
0.28	456 ± 13	/	/

meric particles. A visualization by AFM and SEM of the incorporation of NPs in the microgels is reported below. This complexation causes an increase in the hydrodynamic diameter of the microgels upon addition of NPs (Fig. 1 b), up to a relative size change of $d_{et}/d^0_{et} = 1.8$. Above a weight fraction of NPs of $\chi_{NPs} > 0.3$, we observe aggregation in the samples, presumably induced by hydrophobic attraction between the microgel complexes caused by bridging between the adsorbed NPs, together with aggregation among hydrophobic NP clusters.

We then removed ethanol from the microgels + NPs complexes to characterize the soft particles conformation when the network is dispersed in a good solvent (e.g., pure water at 25°C). This was done by letting the solvent mixture evaporate under vacuum at 40°C, replacing the evaporating solvent with pure water. A confirmation of the ethanol evaporation was obtained by thermogravimetric analysis (Figure S1). Fig. 1 c reports the relative hybrid microgels' size variation with respect to the same particles in water in the absence of NPs (d^0_w). Starting from an initial $d^0_w = 1160 \pm 65$ nm, indicating a fully swollen network, the microgels' size progressively decreases upon increasing the NP concentration (Table 1). Despite the significant size change, the polymer network remains partially swollen for all χ_{NPs} investigated, as indicated by the increased size with respect to complexes at the same χ_{NPs} in water/ethanol mixtures (Table 1). We note that the results in our system are in accordance with previously reported findings [18,19,45]. Microgel size reduction in water upon addition of NPs has been observed in a variety of systems where NPs (of different material, size and surface properties) have been incorporated by in-situ synthesis [14,45], electrostatic adsorption [18,21,23,46] or short-range interactions with the polymer network [19], appearing to be a generic behavior in the case of strong binding and/or bridging between the NPs and the network. In the present work, the hydrophobicity of the NP supports the bridging and formation of additional cross-linking within the microgels. Conversely, in the case of weaker binding, swelling upon NP incorporation is typically observed due to volume effects and an increase in osmotic pressure [8].

Noteworthy, the addition of NPs also influences the microgels' thermal responsiveness, which we quantified measuring the deswelling ratio in water as $d_w(25°C)/d_w(45°C)$. Fig. 1 d shows that the temperature response is progressively decreased upon increasing χ_{NPs}, but still maintained up to $\chi_{NPs} \sim 0.15$. Overall, this indicates that, when dispersed in a good solvent, the incorporation of hydrophobic NPs inside the microgel network causes its partial collapse, decreasing its ability to swell and, consequently, to respond to temperature variations. Interestingly, this complexation has an effect analogous to an *in-situ* increase in crosslinking points within the polymeric networks, as it is achieved by increasing the crosslinker concentration during microgels synthesis. [18,23]

To visualize the distribution of NPs onto the microgels, and gain more information on the network elasticity as a function of NP incorporation, we deposited the microgel + NPs complexes on a solid substrate using the Langmuir-Blodgett technique for AFM and SEM imaging of the particles in the dried state. The microgel + NPs complexes are first prepared in water/ethanol mixture ($\xi_{EtOH} = 0.25$), and are successively spread at the hexane-water interface. A hydrophilic silicon wafer is then lifted through the fluid interface to capture the adsorbed particles (see Materials and Methods for additional details). This procedure ensures a high reproducibility in the particle conformation, avoiding possible differences due to adsorption on the solid substrate either from bulk, or after solvent evaporation, as it can be observed upon drying of a suspension's drop.

Fig. 2a-d reports height (top row) and phase-contrast AFM images (middle row) of microgels without added NPs, and upon increasing the NP concentration. The corresponding height profiles are reported in Fig. 2e. The bare microgels display the standard core-corona profile with a progressive decrease in height from the particle center towards

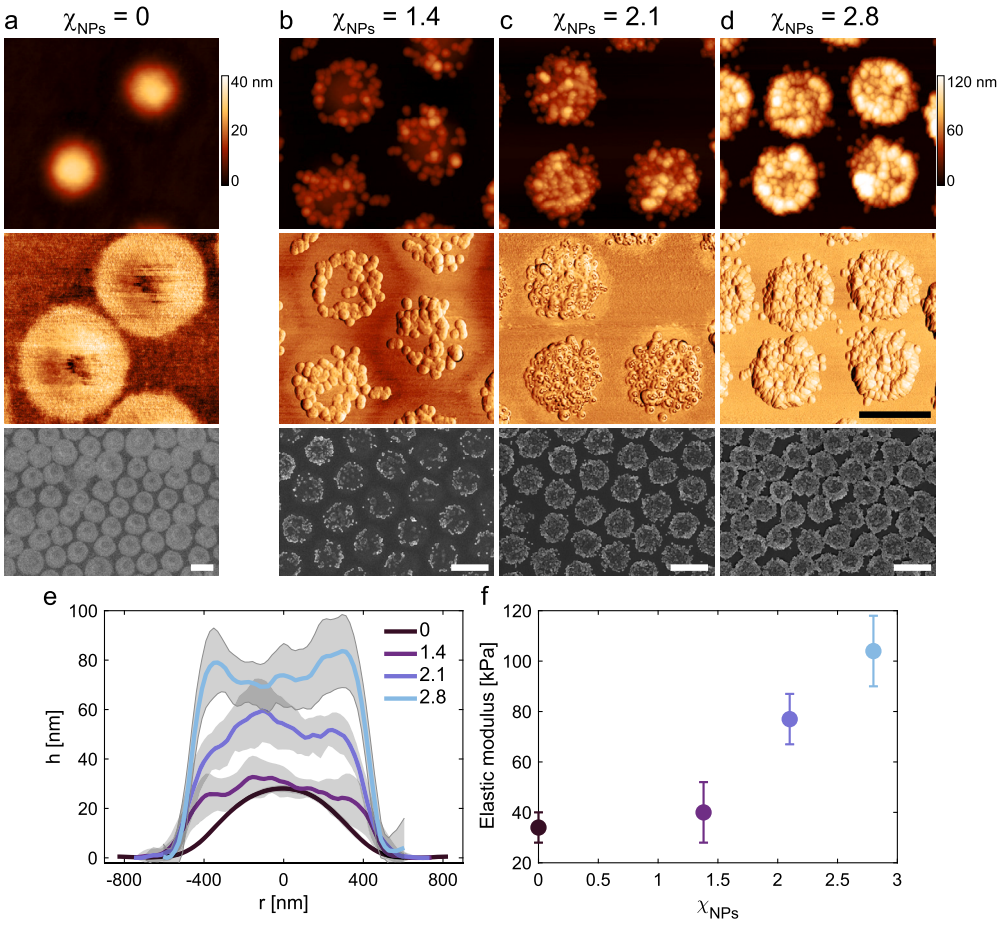

Fig. 2. a-d) AFM height (top row), AFM phase-contrast (middle row) and SEM images of microgels adsorbed at the hexane-water interface and transferred on a silicon wafer. AFM images are obtained in air at room temperature. Scale bar for all images: 1 μm. e) Microgel height profiles extracted from images as in (a-d); the shaded region indicates the standard deviation of the height profiles calculated on at least 10 particles. f) Microgel's elastic modulus obtained from AFM nano-indentation experiments as a function of NP loading. The modulus measurements were carried out in Milli-Q water. (For interpretation of the colors in the figure(s), the reader is referred to the web version of this article.)

its edge, as commonly observed when such particles are transferred on solid substrates from fluid interfaces, with phase-contrast imaging revealing the full spreading on the interface plane [39,43,47,48]. Upon adding the NPs in the mixture, microgel + NPs complexes are formed (Fig. 2 b-d). AFM and SEM imaging shows that increasing the NPs in suspension increases their loading on the microgels, with little to no free NPs visible after transferring from the fluid interface to the solid substrate, even at the highest NPs concentration investigated, corresponding to full coverage of the polymeric particles (Fig. 2 d, see also Figure S2). Interestingly, at low to intermediate NPs concentration (Fig. 2 b, c) the microgels' corona remains visible in the phase-contrast images, indicating that the outer polymer chains are still free to spread on the interface plane despite the presence of the NPs on the microgel surface. Instead, a further increase in NPs loading inside the microgels hinders the reorganization of the polymer network after adsorption and its full spreading at the interface. We note that the actual NP concentration in the hybrids might be slightly lower than their weight ratio used during sample preparation (χ_{NPs}) due to some aggregation of the hydrophobic NPs at high concentration in suspension. Overall, the particle diameter after transferring on the solid substrate decreases from $\sigma = 1.54 \pm 0.3$ μm ($\chi_{NPs} = 0$) to $\sigma = 1.17 \pm 0.2$ μm ($\chi_{NPs} = 2.8$).

We then quantified how the NP incorporation affects the mechanical properties of the hybrid microgels by performing AFM nano-indentation experiments, measured by re-swelling the hybrid microgels in water after particle deposition from the hexane-water interface (see Materials and Methods). As indenter, we used a 2 μm diameter silica colloid attached to a tipless AFM cantilever and measure the compression at the microgels' center (see Materials and Methods). The resulting force versus indentation curves (Figure S3) are therefore mediated by the compression of both the NPs and the polymer network by the AFM colloidal probe. The data in Fig. 2 f indicate a progressive increase in the particles elastic modulus upon NP loading, going from 34 ± 6 kPa to 104 ± 14 kPa for the highest NP concentration investigated. In combination with the DLS data, these results clearly confirm that the complexation of the soft microgels with silica NPs influences the network rigidity and conformation in water, significantly increasing the particle stiffness.

We then explored how the variation in the polymer network stiffness and the presence of NPs influences the hydrophobicity of our hybrid microgels when adsorbed at a fluid interface. To quantify the interfacial conformation of the microgel + NPs complexes we visualized them *in-situ* at the oil-water interface using AFM [37,38]. In particular, imaging from the oil side allows for reconstructing not only the particle stretching on the interface plane, but also the protrusion height (h) and polymer content in the upper oil phase in order to infer on their hydrophobic/hydrophilic character.

For AFM imaging at liquid-liquid interfaces, we used a custom-made AFM fluid-cell setup comprising a thin aqueous layer covered by a droplet of the non-polar phase. We note that the height of the subphase has to be minimal (~ 10 μm) [37] in order to minimize solvent flows that might disturb the image acquisition. When using pure water as the subphase, we could not spread the microgel complexes in wa-

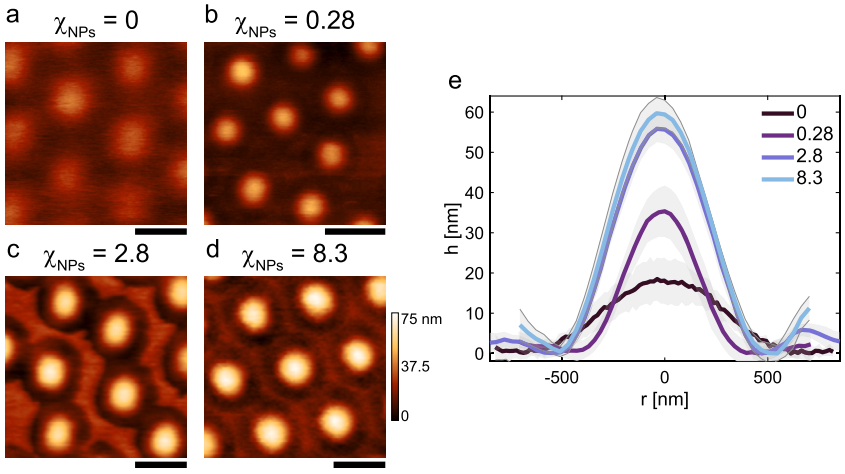

Fig. 3. a-d) *In-situ* AFM imaging at the fluid interface from the hexadecane side (top phase) as a function of NP weight fraction (χ_{NPs}). Bottom phase: water/ethanol mixture ($\xi_{EtOH} = 0.25$); top phase: hexadecane. Scale bar: 1 μm. e) Microgel height profiles in hexadecane as a function of NP weight fraction; the shaded region indicates the standard deviation of the height profiles calculated on at least 10 particles.

ter/ethanol mixture directly at the fluid interface due to dewetting of the underlying aqueous layer. We thus used a water/ethanol mixture at $\xi_{EtOH} = 0.25$ directly as the subphase, while hexadecane was chosen as the upper oil phase. The microgels adsorbed spontaneously at the fluid interface by diffusion during the equilibration time before image acquisition (see Materials and Methods for further details).

We first imaged microgels without NPs (Fig. 3 a). The profile qualitatively matches that of similar microgels adsorbed at a water-hexadecane interface [37]. Despite the partial network collapse due to the presence of ethanol in the subphase, the particle assumes a comparable core-corona structure with the denser core protruding out in the oil phase up to a maximum height of 19 ± 5 nm, and stretching on the interface plane reaching a diameter of about 1 μm. The particles are therefore highly deformed and expanded on the interface plane to decrease the contact between the two fluids until the energy gain from adsorption is balanced by the energy loss from deformation.

Fig. 3 b-d shows images of the hybrid microgels at increasing χ_{NPs}. The absence of visible NPs from the oil side can be attributed to an efficient trapping by the polymeric network that retains the NPs inside the network in contact with an apolar solvent, as well as to a decreased spatial resolution with respect to dry images due to the lateral displacement of mobile polymer chains in contact with the scanning AFM tip. While the profiles remain qualitatively similar, all showing a core-corona conformation with a pronounced deformation on the interface plane (i.e., diameter much larger than the particle height above the interface), quantitative differences can be extracted. In particular, the protrusion height h almost doubles ($h = 35 \pm 6$ nm) for $\chi_{NPs} = 0.28$, reaching a value of 56 ± 3 nm for $\chi_{NPs} = 2.8$, and remaining essentially constant ($h = 58 \pm 4$ nm) upon further NPs addition (Fig. 3 d). The observed increase in polymer content in the oil phase is consistent with an increase in the hydrophobicity of the microgels upon complexation with the NPs, similarly to what reported upon incorporation of polar oils (e.g.: fatty alcohols) inside the polymer network [37,49,50]. A further reason for this increased protrusion might also be the increase in stiffness, as similarly shown for an increase in crosslinking density in standard microgels, as stiffer particles protrude more into the oil phase to maintain a comparable cross-section on the interface plane [37,51]. It is important to remark that the largest part of the microgel protrudes into the underlying water phase. Therefore the profiles in Fig. 3 e strongly differ to the ones in Fig. 2 e, where the overall polymer network + NPs is deposited onto the solid substrate.

Having characterized how the incorporation of hydrophobized NPs inside the microgel network modulates the single-particle stiffness and conformation at the oil-water interface, we turn to investigate how this influences the mechanical response of microgel monolayers. For this aim, we assembled hybrid microgels at a planar hexane-water interface on a Langmuir trough, and recorded the pressure increase upon interfacial compression. Microgels and NPs are first mixed in water/ethanol ($\xi_{EtOH} = 0.25$) and successively spread at the fluid interface. During compression, the microgels are simultaneously transferred onto a silicon wafer that is lifted at a constant speed through the liquid surface. AFM imaging of the dried substrate allows us to relate the surface pressure (Π) measured during the compression experiment with the center-to-center distance (d_{cc}) between the deposited particles (see Materials and Methods for details) [39].

Fig. 4 a-c reports typical AFM images of the monolayers at increasing (Π), for different χ_{NPs}. The resulting compression curves, plotted as Π versus d_{cc} are reported in Fig. 4 d. Interestingly, hybrid microgels at $\chi_{NPs} = 1.4$, which maintain a visible polymer corona and an elastic modulus comparable to that of pure microgels (see Fig. 2), behave similarly to monolayers of microgels without added NPs. The accumulation of NPs within the microgel network does not contribute to the response of the monolayer upon interfacial compression in the range of Π investigated here. We note that comparable results have been reported for different systems composed of standard pNIPAM microgels or microgels without a crosslinked core, both having a similar microgel corona at the interface [43], for which the monolayer mechanical response and structural organization was also comparable, being mostly determined by rearrangements of the outer polymer chains.

Conversely, the addition of a larger number of NPs ($\chi_{NPs} = 2.1$ and 2.8), by decreasing the spreading of the outer microgel corona, shifts the onset of Π increase upon interfacial compression to lower d_{cc} values. In other words, a larger number of microgels is required to cover the interface with a dense monolayer of particles in contact. Nevertheless, a long-range hexagonal assembly is still formed at low Π, regardless of the NP content. A further compression of the interface induces a reorganization of the interfacial microgels, where the microgels with a higher χ_{NPs} see a steeper increase of Π as a function of interfacial compression. This indicates a response that directly depends on the single-particle elasticity and hydrophobicity, as well as on their collective reorganization upon interfacial compression. Additional compression above $\Pi \sim 27$ mN/m of the microgel complexes causes the deposition of a homogeneous layer of NPs where the microgels' centers are no longer discernible, followed by the formation of multilayers, presumably due to monolayer buckling or forced particle desorption from the fluid interface (Figure S4).

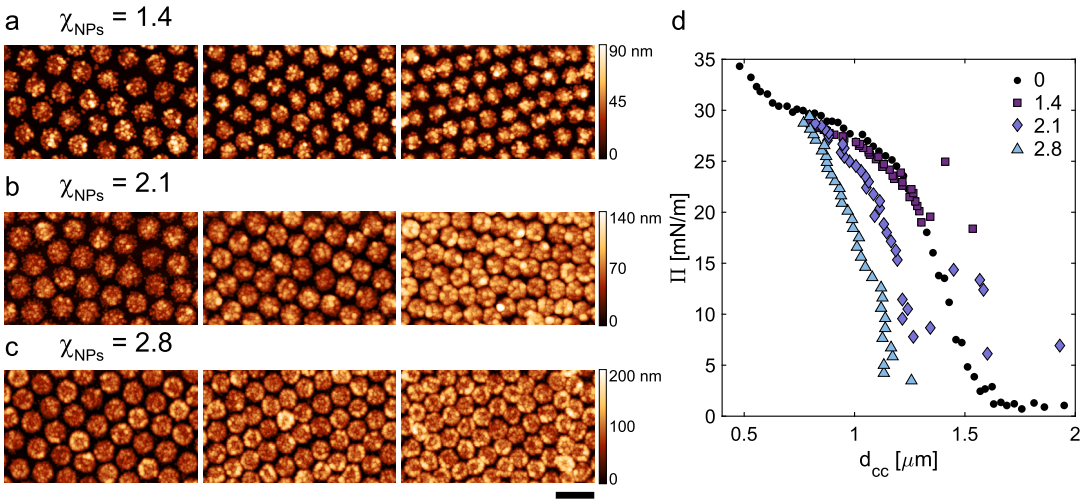

Fig. 4. a-c) AFM height images of the monolayer transferred from the hexane-water interface onto a silicon wafer, at increasing surface pressure (Π), and corresponding decrease of the average center-to-center distance d_{cc}. Samples: a) microgels + NPs, $\chi_{NPs} = 1.4$ ($\Pi = 22.6, 26.3, 27.4$ mN/m); b) microgels + NPs, $\chi_{NPs} = 2.1$ ($\Pi = 7.8, 21.8, 27.0$ mN/m); c) microgels + NPs, $\chi_{NPs} = 2.8$ ($\Pi = 10.6, 24.3, 27.6$ mN/m). Scale bar: 2 μm. d) Compression curves at the hexane-water interface as function of d_{cc} for microgels + NPs complexes at increasing χ_{NPs}.

4. Conclusions

In summary, we present a comprehensive study with a combination of experimental techniques to characterize the incorporation of rigid NPs inside pNIPAM microgels, and their influence on the internal elasticity and resulting 3D conformation after adsorption at a fluid interface. The hybrid microgels are obtained simply by mixing the components in a single fluid phase due to interactions between hydrophobic silica NPs and the collapsed pNIPAM network in water/ethanol mixture at an alcoholic volume fraction of $\xi_{EtOH} = 0.25$. The complexes can then be transferred in water, where the incorporation of NPs causes partial collapse of the swollen pNIPAM network and decreases its ability to respond to temperature variations, similarly to what is reported for a variety of other hybrid microgels characterized by strong binding between the NPs and the polymer [14,18,19,21,23,45,46]. AFM nanoindentation experiments on deposited microgels allow quantifying the increased network stiffness as a function of NPs concentration. When adsorbed at a fluid interface, this results in a decreased spreading of the polymer network on the interface plane, together with an increased hydrophobicity of the hybrid microgels upon increasing χ_{NPs}, with the polymer being located more in the apolar oil phase, as quantified with *in-situ* AFM imaging [37,38].

Finally, we show how the increased single-particle stiffness affects the mechanical response of hybrid microgels monolayers, with stiffer microgels (i.e., higher χ_{NPs}) resulting in a steeper surface pressure slope as a function of interfacial compression. Interestingly, monolayers of hybrid microgels with low χ_{NPs} (1.4 in our case) exhibit compression curves similar to those of pure microgels although their core is significantly stiffer. This hints to the fact that, in this regime, the outer polymer chains alone dictate the mechanical properties of microgel monolayers [43], up to a significant interfacial compression ($\Pi \sim 27$ mN/m in this case).

Overall, these results show that the incorporation of rigid NPs within soft microgels can be used as an efficient post-synthesis way not only to increase the network stiffness, similarly to an increase in the effective crosslinking density, but also to modulate the microgels' hydrophobicity and conformation after adsorption at the fluid interface. We believe therefore that these results expand our current understanding of the superior mechanical properties of hybrid-microgels based materials, such as foams and emulsions [27–29], including biologically relevant ones [31], and may lead to a wealth of new applications, for instance in cosmetics, pharmaceuticals, light-weight materials and catalysis.

CRediT authorship contribution statement

Jacopo Vialetto: Writing – review & editing, Writing – original draft, Visualization, Validation, Resources, Project administration, Methodology, Investigation, Funding acquisition, Data curation, Conceptualization. **Shivaprakash N. Ramakrishna:** Writing – review & editing, Writing – original draft, Visualization, Validation, Methodology, Investigation. **Sebastian Stock:** Writing – review & editing, Writing – original draft, Validation, Methodology, Investigation. **Regine von Klitzing:** Writing – review & editing, Writing – original draft, Supervision, Project administration, Funding acquisition, Conceptualization. **Lucio Isa:** Writing – review & editing, Writing – original draft, Visualization, Supervision, Project administration, Funding acquisition, Conceptualization.

Declaration of competing interest

The authors declare that they have no known competing financial interests or personal relationships that could have appeared to influence the work reported in this paper.

Data availability

Data will be made available on request.

Acknowledgements

The authors thank Simon Scherrer for performing the SEM experiments. J.V. acknowledges funding from the European Union's Horizon 2020 research and innovation programme under the Marie Skłodowska Curie grant agreement 888076 and Ministero dell'Università e della Ricerca (DM 247) - MSCA_0000004, funded by European Union – NextGenerationEU - PNRR, Missione 4 Componente 2 Investimento 1.2. This work is also part of a Collaborative Research Centre funded by the German Research Foundation. Gefördert durch die Deutsche Forschungsgemeinschaft (DFG) - TRR 63 "Integrierte chemische Prozesse in flüssigen Mehrphasensystemen" (Teilprojekt B6) - 56091768.

Appendix A. Supplementary material

Supplementary material related to this article can be found online at https://doi.org/10.1016/j.jcis.2024.05.163.

References

[1] I. Berndt, W. Richtering, Doubly temperature sensitive core-shell microgels, Macromolecules 36 (2003) 8780–8785.

[2] G. Del Monte, D. Truzzolillo, F. Camerin, A. Ninarello, E. Chauveau, L. Tavagnacco, N. Gnan, L. Rovigatti, S. Sennato, E. Zaccarelli, Two-step deswelling in the volume phase transition of thermoresponsive microgels, Proc. Natl. Acad. Sci. 118 (2021) e2109560118.

[3] C.D. Jones, L.A. Lyon, Shell-restricted swelling and core compression in poly(n-isopropylacrylamide) core-shell microgels, Macromolecules 36 (2003) 1988–1993.

[4] D. Lu, M. Zhu, S. Wu, W. Wang, Q. Lian, B.R. Saunders, Triply responsive coumarin-based microgels with remarkably large photo-switchable swelling, Polym. Chem. 10 (2019) 2516–2526.

[5] S.-H. Jung, S. Schneider, F. Plamper, A. Pich, Responsive supramolecular microgels with redox-triggered cleavable crosslinks, Macromolecules 53 (2020) 1043–1053.

[6] M.-C. Tatry, Y. Qiu, V. Lapeyre, P. Garrigue, V. Schmitt, V. Ravaine, Sugar-responsive pickering emulsions mediated by switching hydrophobicity in microgels, J. Colloid Interface Sci. 561 (2020) 481–493.

[7] S. Backes, R. von Klitzing, Nanomechanics and nanorheology of microgels at interfaces, Polymers 10 (2018) 978.

[8] M.U. Witt, S. Hinrichs, N. Möller, S. Backes, B. Fischer, R. von Klitzing, Distribution of CoFe 2 O 4 nanoparticles inside PNIPAM-based microgels of different cross-linker distributions, J. Phys. Chem. B 123 (2019) 2405–2413.

[9] A. Scotti, M.F. Schulte, C.G. Lopez, J.J. Crassous, S. Bochenek, W. Richtering, How softness matters in soft nanogels and nanogel assemblies, Chem. Rev. 122 (2022) 11675–11700.

[10] M. Karg, A. Pich, T. Hellweg, T. Hoare, L.A. Lyon, J.J. Crassous, D. Suzuki, R.A. Gumerov, S. Schneider, I.I. Potemkin, W. Richtering, Nanogels and microgels: from model colloids to applications, recent developments, and future trends, Langmuir 35 (2019) 6231–6255.

[11] M. Ballauff, Y. Lu, "Smart" nanoparticles: preparation, characterization and applications, Polymer 48 (2007) 1815–1823.

[12] M. Karg, T. Hellweg, New "smart" poly(NIPAM) microgels and nanoparticle microgel hybrids: properties and advances in characterisation, Curr. Opin. Colloid Interface Sci. 14 (2009) 438–450.

[13] J. Zhang, S. Xu, E. Kumacheva, Polymer microgels: reactors for semiconductor, metal, and magnetic nanoparticles, J. Am. Chem. Soc. 126 (2004) 7908–7914.

[14] M. Agrawal, A. Pich, S. Gupta, N.E. Zafeiropoulos, J. Rubio-Retama, F. Simon, M. Stamm, Temperature sensitive hybrid microgels loaded with ZnO nanoparticles, J. Mater. Chem. 18 (2008) 2581.

[15] Y. Lu, S. Proch, M. Schrinner, M. Drechsler, R. Kempe, M. Ballauff, Thermosensitive core-shell microgel as a "nanoreactor" for catalytic active metal nanoparticles, J. Mater. Chem. 19 (2009) 3955.

[16] J.-F. Dechézelles, V. Malik, J.J. Crassous, P. Schurtenberger, Hybrid raspberry microgels with tunable thermoresponsive behavior, Soft Matter 9 (2013) 2798.

[17] A.P.H. Gelissen, A. Oppermann, T. Caumanns, P. Hebbeker, S.K. Turnhoff, R. Tiwari, S. Eisold, U. Simon, Y. Lu, J. Mayer, W. Richtering, A. Walther, D. Wöll, 3D structures of responsive nanocompartmentalized microgels, Nano Lett. 16 (2016) 7295–7301.

[18] I. Gorelikov, L.M. Field, E. Kumacheva, Hybrid microgels photoresponsive in the near-infrared spectral range, J. Am. Chem. Soc. 126 (2004) 15938–15939.

[19] K. Gawlitza, S.T. Turner, F. Polzer, S. Wellert, M. Karg, P. Mulvaney, R.V. Klitzing, Interaction of gold nanoparticles with thermoresponsive microgels: influence of the cross-linker density on optical properties, Phys. Chem. Chem. Phys. 15 (2013) 15623.

[20] M. Lehmann, W. Tabaka, T. Möller, A. Oppermann, D. Wöll, D. Volodkin, S. Wellert, R.V. Klitzing, DLS setup for in situ measurements of photoinduced size changes of microgel-based hybrid particles, Langmuir 34 (2018) 3597–3603.

[21] S. Sennato, E. Chauveau, S. Casciardi, F. Bordi, D. Truzzolillo, The double-faced electrostatic behavior of PNIPAm microgels, Polymers 13 (2021) 1153.

[22] M. Boularas, E. Gombart, J.-F. Tranchant, L. Billon, M. Save, Design of smart oligo(ethylene glycol)-based biocompatible hybrid microgels loaded with magnetic nanoparticles, Macromol. Rapid Commun. 36 (2015) 79–83.

[23] F. Brasili, G. Del Monte, A. Capocefalo, E. Chauveau, E. Buratti, S. Casciardi, D. Truzzolillo, S. Sennato, E. Zaccarelli, Toward a unified description of the electrostatic assembly of microgels and nanoparticles, ACS Appl. Mater. Interfaces 15 (2023) 58770–58783.

[24] C. Zhao, G. Yuan, C.C. Han, Stabilization aggregation, and gelation of microsphere induced by thermosensitive microgel, Macromolecules 45 (2012) 9468–9474.

[25] B.S. Hwang, J.S. Kim, J.M. Kim, T.S. Shim, Thermogelling behaviors of aqueous poly(n-isopropylacrylamide-co-2-hydroxyethyl methacrylate) microgel–silica nanoparticle composite dispersions, Materials 14 (2021) 1212.

[26] W. Richtering, Responsive emulsions stabilized by stimuli-sensitive microgels: emulsions with special non-pickering properties, Langmuir 28 (2012) 17218–17229.

[27] T. Watanabe, M. Takizawa, H. Jiang, T. Ngai, D. Suzuki, Hydrophobized nanocomposite hydrogel microspheres as particulate stabilizers for water-in-oil emulsions, Chem. Commun. 55 (2019) 5990–5993.

[28] S. Stock, F. Jakob, S. Röhl, K. Gräff, M. Kühnhammer, N. Hondow, S. Micklethwaite, M. Kraume, R. von Klitzing, Exploring water in oil emulsions simultaneously stabilized by solid hydrophobic silica nanospheres and hydrophilic soft PNIPAM microgel, Soft Matter 17 (2021) 8258–8268.

[29] Y. Nishizawa, T. Watanabe, T. Noguchi, M. Takizawa, C. Song, K. Murata, H. Minato, D. Suzuki, Durable gelfoams stabilized by compressible nanocomposite microgels, Chem. Commun. 58 (2022) 12927–12930.

[30] H. Jiang, L. Liu, Y. Li, S. Yin, T. Ngai, Inverse pickering emulsion stabilized by binary particles with contrasting characteristics and functionality for interfacial biocatalysis, ACS Appl. Mater. Interfaces 12 (2020) 4989–4997.

[31] B.S. Murray, Microgels at fluid-fluid interfaces for food and drinks, Adv. Colloid Interface Sci. 271 (2019) 101990.

[32] H. Jiang, S. Zhang, G. Sun, Y. Li, X. Guan, C. Yang, T. Ngai, Engineering hybrid microgels as particulate emulsifiers for reversible pickering emulsions, Chem. Sci. 13 (2022) 39–43.

[33] Y. Li, S. Zhang, H. Jiang, X. Guan, T. Ngai, Multifunctional silica-modified hybrid microgels templated from inverse pickering emulsions, Langmuir 38 (2022) 6571–6578.

[34] I. Bischofberger, D.C.E. Calzolari, V. Trappe, Co-nonsolvency of PNiPAM at the transition between solvation mechanisms, Soft Matter 10 (2014) 8288–8295.

[35] S. Backes, P. Krause, W. Tabaka, M.U. Witt, D. Mukherji, K. Kremer, R. von Klitzing, Poly(n-isopropylacrylamide) microgels under alcoholic intoxication: when a LCST polymer shows swelling with increasing temperature, ACS Macro Lett. 6 (2017) 1042–1046.

[36] L. Tavagnacco, E. Zaccarelli, E. Chiessi, Molecular description of the coil-to-globule transition of poly(n-isopropylacrylamide) in water/ethanol mixture at low alcohol concentration, J. Mol. Liq. 297 (2020) 111928.

[37] J. Vialetto, S.N. Ramakrishna, L. Isa, In situ imaging of the three-dimensional shape of soft responsive particles at fluid interfaces by atomic force microscopy, Sci. Adv. 8 (2022), eabq2019.

[38] J. Vialetto, F. Camerin, S.N. Ramakrishna, E. Zaccarelli, L. Isa, Exploring the 3D conformation of hard-core soft-shell particles adsorbed at a fluid interface, Adv. Sci. (2023) 2303404, 1-9.

[39] J. Vialetto, N. Nussbaum, J. Bergfreund, P. Fischer, L. Isa, Influence of the interfacial tension on the microstructural and mechanical properties of microgels at fluid interfaces, J. Colloid Interface Sci. 608 (2022) 2584–2592.

[40] S. Stock, A. Schlander, M. Kempin, R. Geisler, D. Stehl, K. Spanheimer, N. Hondow, S. Micklethwaite, A. Weber, R. Schomäcker, A. Drews, M. Gallei, R. von Klitzing, The quantitative impact of fluid vs. solid interfaces on the catalytic performance of pickering emulsions, Phys. Chem. Chem. Phys. 23 (2021) 2355–2367.

[41] M. Rey, M. Ángel Fernández-Rodríguez, M. Steinacher, L. Scheidegger, K. Geisel, W. Richtering, T.M. Squires, L. Isa, Isostructural solid–solid phase transition in monolayers of soft core–shell particles at fluid interfaces: structure and mechanics, Soft Matter 12 (2016) 3545–3557.

[42] B.M. Rey, R. Elnathan, R. Ditcovski, K. Geisel, M. Zanini, M.-A. Fernandez-Rodriguez, V.V. Naik, A. Frutiger, W. Richtering, T. Ellenbogen, N.H. Voelcker, L. Isa, Fully tunable silicon nanowire arrays fabricated by soft nanoparticle templating, Nano Lett. 16 (2016) 157–163.

[43] J. Vialetto, F. Camerin, F. Grillo, S.N. Ramakrishna, L. Rovigatti, E. Zaccarelli, L. Isa, Effect of internal architecture on the assembly of soft particles at fluid interfaces, ACS Nano 15 (2021) 13105–13117.

[44] J.L. Hutter, J. Bechhoefer, Calibration of atomic-force microscope tips, Rev. Sci. Instrum. 64 (1993) 1868–1873.

[45] A. Pich, J. Hain, Y. Lu, V. Boyko, Y. Prots, H.-J. Adler, Hybrid microgels with ZnS inclusions, Macromolecules 38 (2005) 6610–6619.

[46] P.T. Davies, B. Vincent, Uptake of anionic gold nanoparticles by cationic microgel particles in dispersion: the effect of pH, Colloids Surf. A, Physicochem. Eng. Asp. 354 (2010) 99–105.

[47] S. Bochenek, A. Scotti, W. Richtering, Temperature-sensitive soft microgels at interfaces: air–water versus oil–water, Soft Matter 17 (2021) 976–988.

[48] J. Menath, J. Eatson, R. Brilmayer, A. Andrieu-Brunsen, D.M.A. Buzza, N. Vogel, Defined core–shell particles as the key to complex interfacial self-assembly, Proc. Natl. Acad. Sci. 118 (2021) e2113394118.

[49] M. Destribats, V. Lapeyre, E. Sellier, F. Leal-Calderon, V. Schmitt, V. Ravaine, Water-in-oil emulsions stabilized by water-dispersible poly(n -isopropylacrylamide) microgels: understanding anti-finkle behavior, Langmuir 27 (2011) 14096–14107.

[50] X. Guan, Y. Liu, Z. Wan, Y.-L. Steve Tse, T. Ngai, Non-covalent reconfigurable microgel colloidosomes with a well-defined bilayer shell, Chem. Sci. 13 (2022) 6205–6216.

[51] S. Bochenek, F. Camerin, E. Zaccarelli, A. Maestro, M.M. Schmidt, W. Richtering, A. Scotti, In-situ study of the impact of temperature and architecture on the interfacial structure of microgels, Nat. Commun. 13 (2022) 3744.